Generalized design of tunable 3D polarized optical multi-focal spots array[*]

SHI Changkun, XIA Zebin, LÜ Peng, ZHANG Zengqi, and XU Zongwei[**]

State Key Laboratory of Precision Measuring Technology & Instruments, Tianjin University, Tianjin 300072, China

©Tianjin University of Technology 2022

We report a generally designed optical modulation method to garner the tunable three-dimensional (3D) polarized optical multi-focal spots arrays in the focusing system of high numerical aperture (NA) objective lens, and it has good compatibility with vector beams of different polarization states. Based on the vector angular spectrum theory and Fourier transform, the vector light fields of Gaussian beam, Bessel-Gaussian (BG) beam and Laguerre-Gaussian (LG) beam are modulated with the generally designed multi-focal spots phase filter (MSPF). Meanwhile, a generally designed sidelobe suppression transmission (SST) function is employed to reduce the interference effect of the adjacent focal spots in the arrays. Thus, the one-dimensional (1D) axial multi-focal spots array and the 3D multi-focal spots arrays with high spatial resolution can be generated. The MSPF is flexible and reliable in modulating various vector beams, and exhibiting high tunability for the number (3, 12, 21), spacing (4λ—11.3λ) and spatial distribution (1D—3D) of focal spots in the array. With the generally designed MSPF, the generation of multi-focus array is promoted to be more universal and flexible and shows potential application prospects in femtosecond laser multi-beam parallel processing, particle capture, as well as high-density data storage.

In the focusing system of high numerical aperture (NA) objective lens, the tightly focused cylindrical vector light field has aroused wide attention because of its unique focusing characteristics. The research of cylindrical vector light field with inhomogeneous polarization distribution has proposed a novel method to investigate the space-time evolution of light field and the interaction between light and matter. The unique polarization distribution of the cylindrical vector light field in the focusing space has been found with promising applications in quantum information[1,2], optical micromanipulation[3,4], super-resolution microscopy[5,6], micro-nano processing[7,8], as well as high-density optical data storage[9,10]. With the diversification of vector light field modulation methods, the research of multi-focal spots arrays has been extensively conducted, with arbitrary spot locations and numbers in the focal volume[9,11].

Over the past few years, NIE et al[12] presented a method to generate a spherical three-dimensional (3D) super-resolved longitudinal magnetization spot array with a 4π optical microscopic system. In the microscopic system, two high NA objective lenses were used to focus two vectorial beams, respectively, and the 3D arrays could be formed through the interference of the two beams. Moreover, HAO et al[13] proposed a 3D photomagnetic holography based on a conceptual supercritical design. Theoretically, by focusing six coherent circularly polarized beams with two opposite high NA targets, 3D deep super-resolution pure longitudinal magnetization points can be realized in a 4P microscopic system. It is worth noting that the light sources in the relevant researches are all vector beams with fixed polarization states, and most of them are radially polarized Bessel beams. Thus, a general multi-focal spots array optical modulation method that can be applied for different vector light beams seems to be more valuable for the application of multi-focal arrays.

In this study, a generally designed optical modulation method is proposed to generate 3D multi-focal spots arrays. The multi-focal spots phase filter (MSPF) exhibits high compatibility and tunability for different vector light beams, and the number, spacing and spatial distribution of the multi-focal spots array are controllable. Moreover, a sidelobe suppression transmission (SST) function is specially designed to effectively reduce the interference effect of the adjacent focal spots in the arrays, and the spatial resolution of the multi-focal spots array can be improved significantly. After optimized by

the SST, the modulation of the MSPF becomes more stable and reliable for generating the multi-focal spots array, and the multi-focal spots arrays in the focal volume exhibit a high spatial resolution.

Fig.1 presents the schematic diagram of a tightly focused cylindrical vector light field generating the multi-focal spots array. The phase of the cylindrical vector light field in the pupil plane is modulated using an MSPF. Subsequently, the multi-focal spots array can be generated in the focusing space through a high NA objective lens. The geometric focal spots O represent the origin of rectangular coordinates (x, y, z) and cylindrical coordinates (r, φ, z).
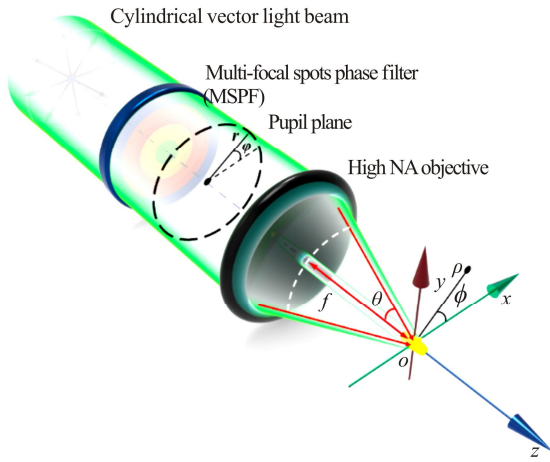

Fig.1 Schematic diagram of multi-focal spots array generated by tightly focused cylindrical vector light beams modulated with an MSPF

Based on the vector diffraction theory, the electric field distribution of the cylindrical vector light beam at the focus is written as

$$E(x,y,z) = \begin{bmatrix} E_x \\ E_y \\ E_z \end{bmatrix} = \frac{-iA}{\pi} \int_0^\alpha \int_0^{2\pi} \sin(\theta) \cos^{1/2}(\theta) \times$$

$$l_0(\theta) \begin{bmatrix} \cos\theta\cos\varphi \\ \cos\theta\sin\varphi \\ \sin\theta \end{bmatrix} e^{ik(r\sin\theta\cos(\varphi-f)+z\cos\theta)} d\theta d\varphi, \quad (1)$$

where A denotes the amplitude constant, θ represents the value of the convergence, $\alpha=\arcsin(NA/n_0)$ is the maximum value of θ, and n_0 expresses the refraction index in free space. The wave number is denoted as $k=2\pi/\lambda$, and λ represents the wavelength of incident laser. $l_0(\theta)$ denotes the amplitude distribution of the cylindrical vector light beam. For the Gaussian beam, Bessel-Gaussian (BG) beam and Laguerre-Gaussian (LG) beam, $l_0(\theta)$ is respectively expressed as

$$l_{0-G}(\theta) = e^{-(\beta_0 \sin\theta/\sin\alpha)^2}, \quad (2a)$$

$$l_{0-BG}(\theta) = e^{-(\beta_0 \sin\theta/\sin\alpha)^2} \cdot J_n(2\beta_0 \sin\theta/\sin\alpha), \quad (2b)$$

$$l_{0-LG}(\theta) = (\beta_0^2 \sin^2\theta/\sin^2\alpha) \cdot e^{-(\beta_0 \sin\theta/\sin\alpha)^2} \times$$
$$L_p^1(2\beta_0^2 \sin^2\theta/\sin^2\alpha), \quad (2c)$$

where β_0 denotes the truncation parameter, expressed as the ratio of the pupil radius to the incident beam waist in front of the high NA objective lens. For the amplitude distribution of BG beam, J_n denotes the Bessel function of the first kind with order n ($n=0$, 1), while L_p^1 represents the generalized Laguerre polynomial with the radial mode number p. In accordance with the Fourier transform theorem, the vector diffraction integral of Eq.(1) is rewritten as the Fourier transform of weighted field. Based on the vector angular spectrum theory, the electric field distribution of multi-focal spots array considering the modulation of MSPF is expressed as[14-16]

$$E(x,y,z) = \frac{-iA}{\pi} \iint T(x,y) \frac{\cos^{1/2}(\theta) l_0(\theta) \vec{e}_{xyz}(\theta,\varphi) e^{ikz}}{\cos\theta} \times$$

$$e^{[-i(f_x x + f_y y)]} df_x df_y = \frac{-iA}{\pi} \times FT[T(x,y)] *$$

$$FT\left[\frac{\cos^{1/2}(\theta) l_0(\theta) \vec{e}_{xyz}(\theta,\varphi) e^{ikz}}{\cos\theta}\right], \quad (3)$$

where the symbol * denotes the convolution operator, and $T(x, y)$ represents the transmission function of the designed MSPF, which is written as

$$T(x,y) = \sum_{b=1}^B [\cos(2\pi x(-x_b + x_0)) - i\sin(2\pi x(-x_b + x_0))] \times$$

$$\sum_{c=1}^C [\cos(2\pi y(-y_c + y_0)) - i\sin(2\pi y(-y_c + y_0))] \times$$

$$\sum_{d=1}^D \exp(\pm ik(z_d - z_0)\cos\theta). \quad (4)$$

The parameters B, C and D represent integers, giving the total number of the prescribed unit focal spots along the x, y and z directions, respectively. Besides, for a multi-focal spots array in plane xy, the parameters B and C are constantly equal. The ranges of b, c and d are (1—B), (1—C) and (1—D), respectively. In the above equation, $(-x_b+x_0)$, $(-y_c+y_0)$ and $(-z_d+z_0)$ denote the lateral and axial displacements, respectively, the parameters x_b, y_c and z_d represent the spatial coordinates in the focal space, and x_0, y_0 and z_0 express the origin of spatial rectangular coordinate system, respectively.

To generate the phase diagram of the multi-focal spots array, the MSPF is adopted to encode the spatial phase of tightly focused vector light beams. Based on the vector diffraction theory, the parameters $n_0=1$, $NA=0.95$, $\lambda=515$ nm are set in Eq.(2), and the truncation parameter β_0 for the Gaussian beam and the BG beam is set to 1. Subsequently, the 1D multi-focal spots arrays are generated with different light sources, and the phase function of 1D multi-focal spots array in the pupil plane is expressed as

$$p(x,y,z) = \sum_{d=1}^D \exp[ik((-x_b + x_0)\sin\theta\cos\varphi +$$

$$(-y_c + y_0)\sin\theta\sin\varphi + (-z_d + z_0)\cos\varphi)]. \qquad (5)$$

The design parameters of 1D arrays are $(0, 0, 10\lambda)$, $(0, 0, 0)$, $(0, 0, -10\lambda)$. Fig.2(a1—b2) present the electric fields of radially and azimuthally polarized Gaussian beam and BG beam in the focal volume, respectively. The position of the electric field intensity taken is illustrated by the white dotted line to investigate the electric filed intensity of the focal spots in the array. Notably, due to the non-diffraction characteristics of BG beam, the interference effect of BG beam is significantly weaker than that of Gaussian beam, while the electric field intensity of the middle focal spots remains higher than 98% (Fig.2(c1—c2)) in the 1D array. For the multi-focal spots array generated by the radially polarized Gaussian beam, the transverse resolution is 0.75λ and the longitudinal resolution is 1.4λ, while for the azimuthally polarized Gaussian beam, the transverse resolution is 1.32λ and the longitudinal resolution is 1.5λ. Compared with the Gaussian beam, the transverse resolution of the radially polarized BG beam is 0.67λ and the longitudinal resolution is 1.4λ, while the transverse resolution of the azimuthally polarized is 1.26λ and the longitudinal resolution is 1.5λ.
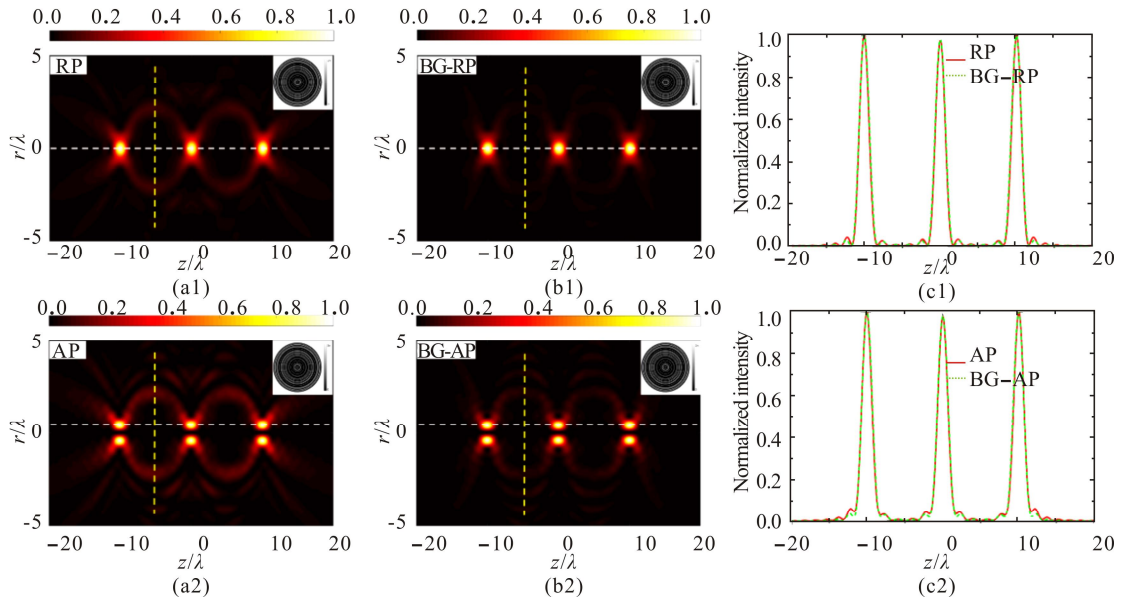

Fig.2 Normalized intensity distributions in the focal region of 1D multi-focal spots vector light field arrays modulated by the MSPF (Insets are phase diagrams of the array): (a1-a2) 1D multi-focal spots vector light field arrays of the radially and azimuthally polarized Gaussian beams; (b1-b2) 1D multi-focal spots vector light field arrays of the radially and azimuthally polarized BG beams; (c1-c2) Normalized intensities of the 1D multi-focal spots array

For the high spatial resolution multi-focal spots arrays generated under general tightly focusing conditions, it is required to have clear array distribution and morphology characteristics in the focusing space, which means that the interference light intensity region generated between adjacent focal points in the multi-focal spots array should not affect the light field distribution of the multi-focal spots array. However, compared with the BG vector beam, the interference effect between adjacent focal spots in the multi-focal spots array produced by the Gaussian vector light field is clearly visible, which cannot meet the general design requirements of MSPF. In order to make the MSPF can be better applied to different incident light sources and achieve high resolution multi-focal spots array. Here, a multi-stage sidelobe electric field suppression transmittance function SST is designed to reduce the intensity and the range of the multi-stage sidelobe electric field. SST is coupled with the MSPF, and the interference effect of adjacent focal points in the multi-focal spots array is suppressed during the realization of multi-focus array, so as to obtain the multi-focal spots array with clear structure. The equation of the SST is written as

$$\text{SST}(\theta) = \sin(k_1\pi\sin\theta/(2\alpha)^2). \qquad (6)$$

Under tight focusing condition, the focal spot in the array is dominated by the interference of the nearest focal spot. As a result, according to the multi-beam interference theory, the electric field in the interference region can be expressed as

$$I_{i-(x,y,z)} = E_{i-L_i} \cdot E_i + E_i \cdot E_{i-R_i} + E_{i-L_i} \cdot E_{i-R_i}, \qquad (7)$$

where the i-(x, y, x) represent the focal spots along the x, y or z direction, and x' and y' correspond to z and r in the rz plane, respectively. E_i is the electric field distribution of the selected central focal spot, and E_{i-Li} and E_{i-Ri} represent the electric field distributions of the nearest neighbor focal spots to the left and right of the central focus, respectively. In the multi-focal spot arrays, each focal spot can be equivalent to a point light source in the focal space, and the interference of focal spots in multi-focal spot array

mainly comes from the adjacent one. Therefore, the interference intensity coefficient ξ is pre ferred to quantitatively analyze the interference effect in the multi-focal spots array, and ξ can be expressed as

$$\xi = (N\sum_{i=1}^{N} E_i \cdot E_{ad-i}) / (\sum_{i=1}^{N} |E_i|^2), \qquad (8)$$

where E_i and E_{ad-i} represent the electric field distributions of the focal spot and the adjacent focal spot in the array, respectively. N is the number of the focal spots in the array, and the ranges of i and ad are (1−N). Combining Eqs.(7) and (8), the normalized interference electric field in the multi-focal spots array and the maximum value of the interference intensity coefficient in the interference region can be obtained. Before optimized by SST, the maximum values of ξ for radially and azimuthally polarized Gaussian beams are 0.57 and 0.774, respectively, and those for the radially and azimuthally polarized BG beams are 0.28 and 0.086, respectively. By contrast, after optimized by SST, the maximum values of ξ for radially and azimuthally polarized Gaussian beams are 0.026 and 0.14, respectively, and those for the radially and azimuthally polarized BG beams are 0.075 and 0.017, respectively. For the multi-focal spots array, we expect the electric field strength in the interference region to be as small as possible to make the distribution of the multi-focal array with high spatial resolution. Therefore, based on the results of the interference intensity coefficient, we expect that the maximum electric field strength of the interference region in the electric field should not exceed 0.15, so we further analyzed the electric field strength of the interference region in the normalized electric field.

In the normalized electric field of the multi-focal spots array, before optimized by SST, the maximum electric field intensity of the radially polarized Gaussian beam in the region of the interference electric field (marked by the dotted yellow line) is 0.08, the azimuthally polarized Gaussian beam is 0.12, and the radially and azimuthally polarized BG beams are 0.025 and 0.046, respectively. However, after optimized by SST, the maximum interference electric field intensity of the radially polarized Gaussian beam is 0.016, the azimuthally polarized Gaussian beam is 0.03, and the radially and azimuthally polarized BG beams are 0.011 and 0.028, respectively. As we can see, the SST obviously inhibits the electric field in the interference region.

When the parameter k_1 is set to 0.15, SST serves as an additional factor, similar to a multi-stage sidelobe electric field attenuation filter, and each focal-spot in the array can be modulated. According to Fig.3(a1—b2), the 1D multi-focal spots arrays modulated with the SST show high structural resolution, and the interference effect of the adjacent focal spot in 1D arrays is reduced significantly. Interestingly, the electric intensity of the tightly focused vector polarized Gaussian beams has a quasi-non-diffraction characteristic, and the distribution of 1D array's electric field garnered with vector polar-

ized Gaussian beam is nearly indistinguishable from that of the vector polarized BG beam. Obviously, the effect arising from SST on the interference effect of the adjacent focal spot is more significant in the Gaussian beams, and the electric field intensity of the focal spot in the arrays still maintains a high electric intensity, the normalized intensity remains higher than 98% (Fig.3(c1—c2)). For the multi-focal spots array generated by the radially polarized Gaussian beam, the transverse resolution is 0.62λ and the longitudinal resolution is 1.4λ, while for the azimuthally polarized Gaussian beam, the transverse resolution is 1.22λ and the longitudinal resolution is 1.4λ. Compared with the Gaussian beam, the transverse resolution of the radially polarized BG beam is 0.58λ and the longitudinal resolution is 1.5λ, while the transverse resolution of the azimuthally polarized beam is 1.18λ and the longitudinal resolution is 1.5λ. As we expected, the SST is capable of effectively reducing the interference effect of the adjacent focal spots in multi-focal spots arrays, the transverse resolution is significantly improved, whereas it has no effect on the central electric intensity of the focal spot in the array.

According to Eqs.(4) and (5), the electric field distribution in the focusing space can be determined by solving the convolution of Fourier transform, and the spatial phase of the multi-focal spots array is expressed as

$$p(x, y, z) = \sum_{b=1}^{B}\sum_{c=1}^{C}\sum_{d=1}^{D} \exp[ik((-x_b + x_0)\sin\theta\cos\varphi +$$
$$(-y_c + y_0)\sin\theta\sin\varphi + (-z_d + z_0)\cos\varphi)]. \quad (9)$$

Based on the pure-phase modulation of MSPF, a 3D multi-focal spots array is designed with different structures (e.g., "T", "J" and "U"), and the MSPF is adopted to modulate radially and azimuthally polarized Gaussian beam and BG beam, respectively. Tab.1 lists the design parameters of the 3D multi-focal spots array.

Fig.4(c) represents the phase diagram of the 3D multi-focal spots array "TJU", and Fig.4(a1—b2) show the 3D multi-focal spots arrays generated with radially and azimuthally polarized Gaussian beam and BG beam in the focal space, respectively. The transverse and longitudinal resolutions of 3D multi-focal spots arrays have no significant change compared with 1D multi-focal spots arrays, and in the normalized electric field of the 3D multi-focal spots arrays optimized by SST, the interference intensity coefficients ξ of all the vector light beams in different z- layers do not exceed 0.15. In the 3D multi-focal spots arrays "TJU", the minimum spacing of the adjacent focal spots is 4.2λ, and the maximum spacing of the adjacent focal spots is 6λ. The 2D arrays "T", "J" and "U" of 3D multi-focal spots array generated with radially and azimuthally polarized Gaussian beams still exhibit a quasi-non-diffraction characteristic. Obviously, the design of the SST is found to be effective to reduce the interference effect of the adjacent focal spots in the arrays to maintain a spatial resolution, while showing high compatibility with various vector beams.
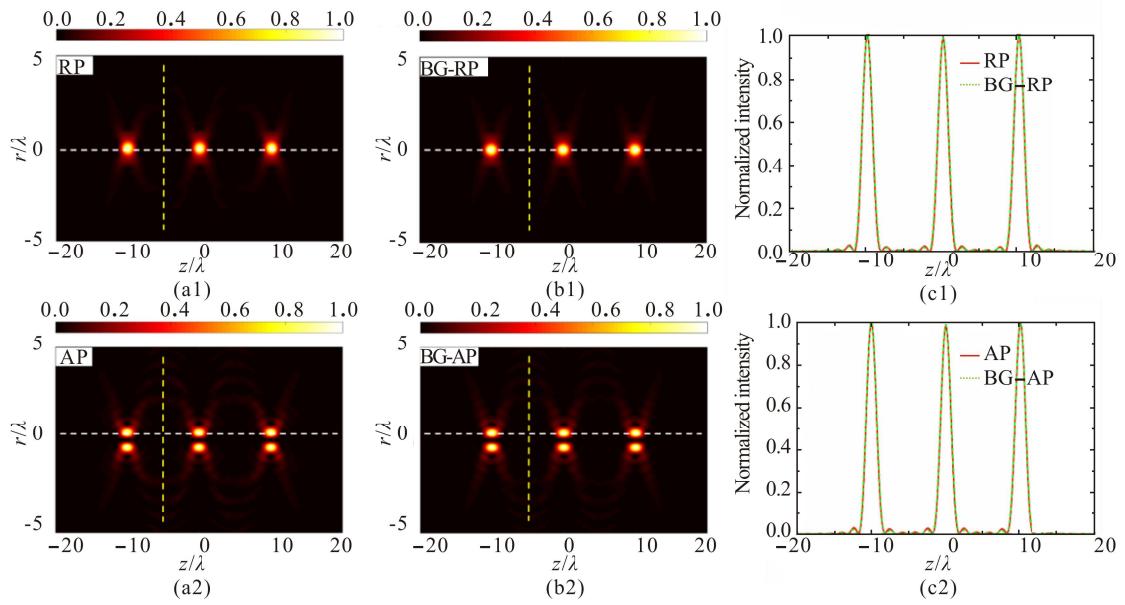
Fig.3 Normalized intensity distributions in the focal region of 1D multi-focal spots vector light field arrays optimized by the SST: (a1-a2) 1D multi-focal spots vector light field arrays of the radially and azimuthally polarized Gaussian beams; (b1-b2) 1D multi-focal spots vector light field arrays of the radially and azimuthally polarized BG beams; (c1-c2) Normalized intensities of the 1D multi-focal spots array optimized with SST

Tab.1 Design parameters of 3D arrays "TJU"

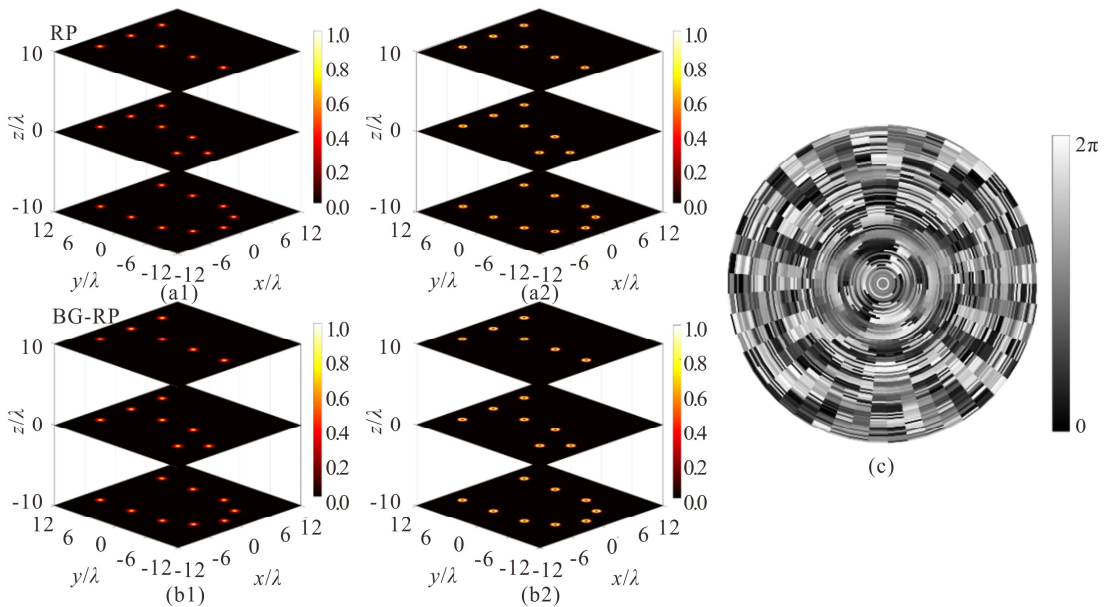| Arrays	T	J	U
(x_b, y_c)	$(6\lambda, 9\lambda)$, $(0, 9\lambda)$, $(0, 3\lambda)$, $(0, -3\lambda)$, $(0, -9\lambda)$, $(-6\lambda, 9\lambda)$	$(6\lambda, 9\lambda)$, $(0, 9\lambda)$, $(0, 3\lambda)$, $(0, -3\lambda)$, $(3\lambda, -9\lambda)$, $(-6\lambda, -6\lambda)$, $(-6\lambda, 9\lambda)$	$(6\lambda, 9\lambda)$, $(6\lambda, 3\lambda)$, $(6\lambda, -3\lambda)$, $(4\lambda, -7\lambda)$, $(0, -9\lambda)$, $(-4\lambda, -7\lambda)$, $(-6\lambda, 9\lambda)$, $(-6\lambda, 3\lambda)$, $(-6\lambda, -3\lambda)$
(x_0, y_0, z_0)	$(0, 0, 0)$	$(0, 0, 0)$	$(0, 0, 0)$
z_d	10λ	0	-10λ

Fig.4 3D multi-focal spots arrays "TJU" generated with the Gaussian beam and BG beam: (a1-b1) 3D multi-focal spots arrays "TJU" generated with the radially polarized Gaussian beam and BG beam; (a2-b2) 3D multi-focal spots arrays "TJU" generated with the azimuthally polarized Gaussian beam and BG beam; (c) Phase diagram of the 3D multi-focal spots array "TJU"

Considering the diversity of the applications for the multi-focal spots arrays, the 3D optical cage system generated by the radially polarized LG beam is further investigated. For the radially polarized LG beam, the truncation parameter β_0 of LG beam is set as 1.26. Based on the generally designed multi-focal spots filter MSPF, the 1D optical cage array along the optical axis is garnered at first. Fig.5(a1—a2) present the 1D optical cage arrays generated with the radially polarized LG beam. For the multi-focal spots array generated by the radially polarized LG beam, the transverse resolution of the single optical cage in the 1D array is 1.95λ, and the longitudinal resolution is 3.25λ. In the normalized interference electric field of the 1D multi-focal spots array, before optimized by SST, the maximum value of the interference intensity coefficient ξ is 0.99. However, after optimized by SST, the maximum value of ξ for radially polarized LG beam is 0.059. By contrast, in the normalized electric field of the multi-focal spots array generated by the radially polarized LG beam, the maximum intensity of the interference region is 0.16. After optimized by SST, the transverse and longitudinal resolutions of the single optical cage are 1.88λ and 3.34λ, respectively, and the maximum intensity of the interference region decays to 0.05. Compared with the distribution of electric fields presented in Fig.5(a1—a2), the spatial resolution of 1D multi-focal spots optical cage array optimized by the SST is significantly higher than the array shown in Fig.5(a1) that is not optimized. With the reduction of the multi-stage sidelobe electric field, the shape of the focal spots in the array evolves into a shape of light shell.

For the 3D cubic multi-focal spots optical cage array, the parameters of the 3D array are listed in Tab.2, and the phase diagram of the 3D cubic multi-focal spots optical cage array is the same as Fig.2.

Tab.2 Design parameters of 3D multi-focal spots optical cage arrays

Arrays	2×2	2×2	2×2
(x_b, y_c)	$(-4\lambda, -4\lambda)$, $(-4\lambda, 4\lambda)$, $(4\lambda, -4\lambda)$, $(4\lambda, 4\lambda)$	$(-4\lambda, -4\lambda)$, $(-4\lambda, 4\lambda)$, $(4\lambda, -4\lambda)$, $(4\lambda, 4\lambda)$	$(-4\lambda, -4\lambda)$, $(-4\lambda, 4\lambda)$, $(4\lambda, -4\lambda)$, $(4\lambda, 4\lambda)$
(x_0, y_0, z_0)	$(0, 0, 0)$	$(0, 0, 0)$	$(0, 0, 0)$
z_d	10λ	0	-10λ

Fig.5(c) presents the normalized electric field distribution of the 3D cubic multi-focal spots optical cage array, the transverse and longitudinal resolutions of 3D multi-focal spots optical cage array have no significant change compared with 1D multi-focal spots optical cage array, and in the 3D multi-focal spots optical cage array, the interference intensity coefficients ξ of the radially polarized LG beams in different z-layers do not exceed 0.15. The 2D multi-focal spots optical cage array along z-axis in the 3D array is recognized as a 2×2 multi-focal spots array, and the spacing of the adjacent focal spots is 8λ. For the cross sections $x=-4\lambda$ and $y=x$, the transverse spacings of the adjacent focal spots are 8λ and 11.3λ, respectively. With the increase in the spacing, the interference effect of the adjacent 1D multi-focal spots arrays is reduced, and no significant interference effect is found between the adjacent focal spots in the array. The generally designed MSPF, after optimized with the SST, shows high compatibility with various vector light beams, while showing high tunability for the number, spacing and spatial distribution of focal spots in the array.
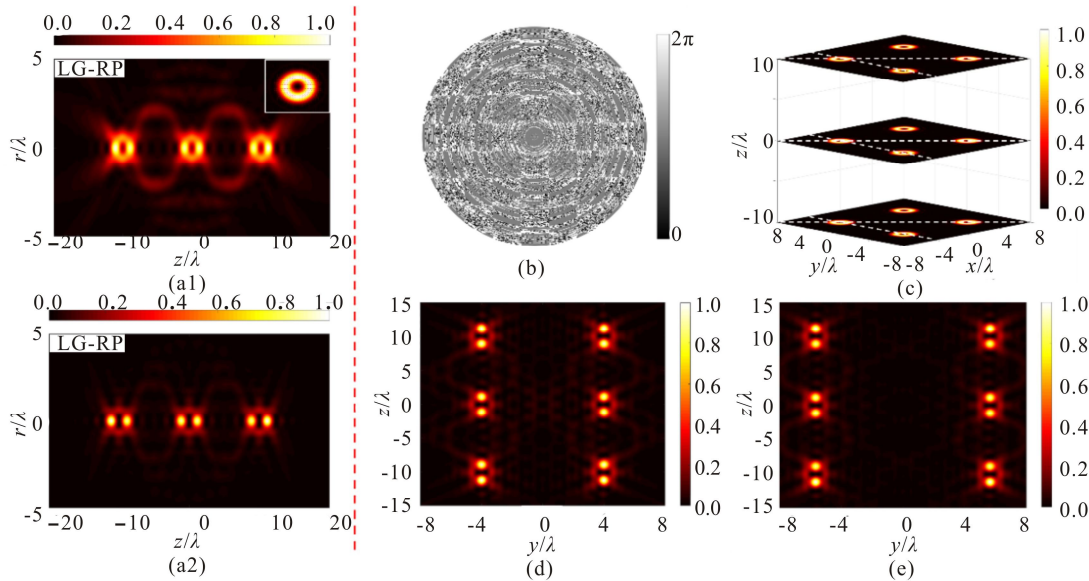

Fig.5 Multi-focal spots arrays generated with the radially polarized LG beam: (a1-a2) Normalized intensity distributions of 1D multi-focal spots arrays without and with SST optimization; (b) Phase diagram of the 3D multi-focal spots array; (c) 3D multi-focal spots arrays generated with the radially polarized LG beam; (d) 2D multi-focal spots arrays in cross section ($x=-4\lambda$) of 3D multi-focal spots arrays; (e) 2D multi-focal spots arrays in cross section ($y=x$) of 3D multi-focal spots arrays

In summary, a generally designed multi-focal spots phase filter is proposed to generate tunable 3D polarized optical multi-focal spots arrays in the focusing system of high NA objective lens. Moreover, an SST function is applied to the MSPF to reduce the interference effect of the adjacent focal spots in the arrays. For the 1D axial multi-focal spots array and the 3D multi-focal spots arrays garnered with different light sources in the focal volume, the MSPF exhibits high flexibility, and the number and the position of the multi-focal spots array are controllable. By combining the SST, the interference effect of the adjacent focal spots in the multi-focal spots array is significantly inhibited. The novel method has high compatibility with various vector light beams, while showing high tunability for the number, spacing and spatial distribution of focal spots in the array. In the future, the proposed method can be extensively used in the research of super-resolution fluorescence imaging, ultrafast laser multi-beam parallel processing, high-density data storage and optical manipulation.

Statements and Declarations

The authors declare that there are no conflicts of interest related to this article.

References

[1]   LI Z X, RUAN Y P, CHEN P, et al. Liquid crystal devices for vector vortex beams manipulation and quantum information applications[J]. Chinese optics letters, 2021, 19：112601.

[2]   YAO A M, PADGETT M J. Orbital angular momentum：origins, behavior and applications[J]. Advances in optics and photonics, 2011, 3：161-204.

[3]   ZHANG Y, WANG M, NING Z, et al. Temporal effect on tight focusing, optical force and spin torque of high-order vector-vortex beams[J]. Optics & laser technology, 2022, 149：107844.

[4]   SONG X. Three-dimensional optical bottle beams for axial optical tweezers based on interference of Bessel beams[C]//Optical Trapping and Optical Micromanipulation XVIII, August 1-5, 2021, San Diego, California, USA. Bellingham：International Society for Optics and Photonics, 2021：117982J.

[5]   ZHANG Y, LIU X, LIN H, et al. Ultrafast multi-target control of tightly focused light fields[J]. Opto-electronic advances, 2021：76-87.

[6]   KOZAWA Y, SAKASHITA R, UESUGI S S. Imaging with a longitudinal electric field in confocal laser scanning microscopy to enhance spatial resolution[J]. Optics express, 2020, 28.

[7]   LI Y, HONG M. Parallel laser micro/nano‑processing for functional device fabrication[J]. Laser & photonics reviews, 2020, 14：1900062.

[8]   XIAO G, HE Y, LIU S, et al. Laser processing of micro/nano biomimetic structures[J]. Micro & nano letters, 2021, 16：327-335.

[9]   LAN T H, TIEN C H. Servo study of radially polarized beam in high numerical aperture optical data storage system[J]. Japanese journal of applied physics, 2007, 46(6B)：3758-3760.

[10]   LUO J, ZHANG H, WANG S, et al. Three-dimensional magnetization needle arrays with controllable orientation[J]. Optics letters, 2019, 44(4)：727-730.

[11]   YU Y, HUANG H, ZHOU M, et al. Creation of a multi-segmented optical needle with prescribed length and spacing using the radiation pattern from a sectional-uniform line source[J]. Scientific reports, 2017, 7：1-5.

[12]   NIE Z Q, LIN H, LIU X F, et al. Three-dimensional super-resolution longitudinal magnetization spot arrays[J]. Light：science & applications, 2017, 6：e17032.

[13]   HAO C, NIE Z, YE H, et al. Three-dimensional super-critical resolved light-induced magnetic holography[J]. Science advances, 2017, 3：e1701398.

[14]   RICHAEDS B, WOLF E. Electromagnetic diffraction in optical systems II. Structure of the image field in an aplanatic system[J]. Proceedings of the Royal Society A, 1959, 253：358-379.

[15]   KOZAWA Y, SATO S. Focusing of higher-order radially polarized Laguerre-Gaussian beam[J]. Journal of the Optical Society of America A, 2012, 29：2439-2443.

[16]   LEUTENEGGER M, RAO R, LEITGEBR A, et al. Fast focus field calculations[J]. Optics express, 2006, 14：11277-11291.